Influence of suture size on the frictional performance of surgical suture evaluated by a penetration friction measurement approach

Zhang, Gangqiang; Zeng, Xiangqiong; Su, Yibo; Borras, F. X.; de Rooij, Matthijn B.; Ren, Tianhui; van der Heide, Emile

DOI
10.1016/j.jmbbm.2018.02.003

Publication date
2018

Document Version
Final published version

Published in
Journal of the Mechanical Behavior of Biomedical Materials

Journal of the Mechanical Behavior of Biomedical Materials 80 (2018) 171–179

Contents lists available at ScienceDirect

Journal of the Mechanical Behavior of Biomedical Materials

journal homepage: www.elsevier.com/locate/jmbbm

Influence of suture size on the frictional performance of surgical suture evaluated by a penetration friction measurement approach

Gangqiang Zhang[a,b], Xiangqiong Zeng[b,c], Yibo Su[d], F.X. Borras[b], Matthijn B. de Rooij[b], Tianhui Ren[a,*], Emile van der Heide[b,e,f]

[a] Shanghai Jiao Tong University, School of Chemistry and Chemical Engineering, Key Laboratory for Thin Film and Microfabrication of the Ministry of Education, 200240, Shanghai, China
[b] University of Twente, Laboratory for Surface Technology and Tribology, 7500AE Enschede, The Netherlands
[c] Chinese Academy of Sciences, Shanghai Advanced Research Institute, Lubricating Materials Laboratory, 201210 Shanghai, China
[d] Brightlands Materials Center, Urmonderbaan 22 6167 RD Geleen, The Netherlands
[e] TU Delft, Faculty of Civil Engineering and Geosciences, Stevinweg 1, 2628 CN Delft, The Netherlands
[f] Ghent University, Soete Laboratory, Technologiepark Zwijnaarde 903, B-9052 Zwijnaarde, Belgium

ARTICLE INFO

Keywords:
Penetration friction
Surgical suture
Normal force
Skin substitute
Penetration contact model

ABSTRACT

The frictional performances of surgical sutures have been found to play a vital role in their functionality. The purpose of this paper is to understand the frictional performance of multifilament surgical sutures interacting with skin substitute, by means of a penetration friction apparatus (PFA). The influence of the size of the surgical suture was investigated. The relationship between the friction force and normal force was considered, in order to evaluate the friction performance of a surgical suture penetrating a skin substitute. The friction force was measured by PFA. The normal force applied to the surgical suture was estimated based on a Hertzian contact model, a finite element model (FEM), and a uniaxial deformation model (UDM).

The results indicated that the penetration friction force increased as the size of the multifilament surgical suture increased. In addition, when the normal force was predicted by UDM, it was found that the ratio between the friction force and normal force decreased as the normal force increased. A comparison of the results suggested that the UDM was appropriate in predicting the frictional behavior of surgical suturing.

1. Introduction

Suturing is a fundamental surgical skill that must be acquired and improved upon by any practitioner in surgery (Misra et al., 2008). The frictional performance of surgical suture-tissue interaction is an important factor in determining the success of suturing. Generally, if high friction occurs during interactions between surgical sutures and tissues, the sliding of the surgical suture might cause “secondary trauma” to soft or fragile tissue, such as the eye, liver and blood vessels. Moreover, in cosmetic cutaneous surgery, suturing trauma on the face should be rigorously avoided (Bloom and Goldberg, 2007). Furthermore, an understanding of the frictional parameters of surgical sutures can provide objective guidance for surgeons. Therefore, it is essential to investigate the frictional performance of suture-tissue interaction through a simulation of suturing.

The coefficient of friction (COF), defined as the quotient of the friction force and the normal force, is a significant factor in understanding the friction performance of surgical sutures. It is found that textile materials do not obey Amontons’ law of friction (Gralen, 1952; Ramkumar et al., 2003, 2004). This law explains why frictional performance is successful for materials that deform elastically but fails for textile materials, e.g, because of viscoelastic deformation (Ghosh et al., 2008).

The frictional performance of fibrous materials is typically evaluated by one of the two following methods: the capstan method (Gao et al., 2015; Robins et al., 2000; Tu and For, 2004; Tu and Fort, 2004) and the twist method (El Mogahzy and Gupta, 1993a; Gralén et al., 1953a; Gralen and Lindberg, 1948; McBride, 1965). The capstan method and twist method are also used to evaluate the frictional performance of surgical sutures sliding on the tissue surface (Gupta et al., 1985; Zhang et al., 2017b). However, these fibre-to-fibre or fibre-to-metal friction models could not simulate the suturing process because the operational and contact conditions differ. In the suturing process, the needle penetrates the tissue and creates a freshly formed counter surface with a damaged tissue. The diameter of the needle is slightly larger than that of the suture, which results in spring-back and

* Corresponding author.
E-mail address: thren@sjtu.edu.cn (T. Ren).

https://doi.org/10.1016/j.jmbbm.2018.02.003
Received 8 October 2017; Received in revised form 20 January 2018; Accepted 2 February 2018
Available online 03 February 2018
1751-6161/

subsequent normal force over the circumference of the suture. Hence, the sliding contact between the suture and tissue is not restricted to surface phenomena but might also lead to deformations beneath the surface layer. In addition, the normal force acting on the surgical suture in a suturing process is different from the frictional conditions of the capstan and twist methods.

The purpose of this study is to investigate the influence of suture size on the frictional performance of multifilament surgical suture-skin substitute interactions, with respect to the relationship between friction force and normal force. A penetration friction apparatus (PFA) (Zhang et al., 2017a) was developed to investigate the friction force of suture - tissue interaction in a representative way. In this study, the normal force was estimated by a Hertzian contact model, a finite element model (FEM) and a uniaxial deformation model (UDM). In the stitching process, the normal force is the elastic deformation force of tissue with a perpendicular direction to the motion. The PFA uses the same principle to apply the normal force. This is the first time this subject has come under discussion, namely, the relationship between friction force and normal force when a surgical suture penetrates a skin substitute. This information can provide a reference for practitioners, enhance the efficiency of suturing and offer formal suture training skills.

2. Methods

2.1. Measurement of friction force

2.1.1. Materials

The frictional performance of a surgical suture is influenced by mechanical and surface properties as well as by operational conditions. For better assistance with PFA, PGA multifilament surgical suture, skin substitute (silicone rubber) and straight stainless steel tapered needles were used in this study.

Polyglycolic acid (PGA) multifilament surgical sutures (Weihai Weigao Medical Instruments Co., Ltd) were selected for this study. The multifilament surgical sutures with a twist structure and rough surface show high friction properties. The related properties of PGA multifilament surgical sutures are listed in Table 1.

In order to control the frictional procedure and to be able to compare the friction results in a non-medical environment, skin substitute is used in this work to simulate human skin. This is because skin substitutes have the advantages of long-term stability, lower cost, easy storage and manipulation and better control over their physical properties than skin. In addition, the use of skin substitutes lacks the ethical issues that are connected to the use of skin. Moreover, silicone rubbers have a somewhat higher modulus, a lower rate of strain hardening and a comparable toughness (Shergold and Fleck, 2005). This is in reasonable agreement with Oliver et al. (Shergold et al., 2006). The skin substitute is sil8800 (Red, 80 IRHD) with a shear modulus of 2.7 MPa (Shergold and Fleck, 2005).

Straight stainless steel tapered needles (Weihai Weigao Medical Instruments Co. Ltd.) with a silicone coating were used. These needles contain a swaged attachment end attached to the surgical suture, as shown in Fig. 1. This type of needle used for skin closure in some surgeries has a sharp tip with smooth edges and is less traumatic to the surrounding tissues. Moreover, the straight needle can be extended beyond the skin vertically. The motion of the surgical suture is in accordance with the model of PFA. A needle with a swaged attachment end provides a virtually step-free transition from thread to needle thus reducing tissue trauma.

Table 1
Parameters of surgical sutures.

Items	Size	Diameter (mm)
PGA multifilament surgical suture	1 #	0.55
	0 #	0.46
	2-0	0.34
	3-0	0.23
	4-0	0.19

Fig. 1. Schematic illustration of straight stainless steel tapered needle.

In the suturing process, the diameter of the surgical needle is larger than the diameter of the surgical suture. Hence, friction force is generated only during the penetration procedure of a surgical suture. When the surgical suture slides vertically through the skin substitute, meaning that the penetration angle is 90°, the value of the force measured by the PFA is equal to the value of the friction force.

Prior to the experiments, the surgical suture was cut into samples of 25 cm in length. Circular-shaped skin substitute samples were made 2 mm thick, with a diameter of 23 mm. The circular skin substitute samples were ultrasonically cleaned in acetone, isopropanol and finally water, each time for 10 min.

2.1.2. Tribological measurement

The PFA was used to investigate the frictional performance of a surgical suture penetrating tissue substitute. This apparatus was introduced in a previous work (Zhang et al., 2017a). The major components of the PFA are a dedicated sample gripper and an angle adjuster, as shown in Fig. 2. In the sample gripper, a chamber is drilled so allow the treated skin substitute to be inserted. Furthermore, a cross hole was set in the middle of the top and bottom holder of the sample gripper.

The sample gripper was set in a Zwick/Roell 500 N tensile tester, as shown in Fig. 3. Two steps were included in this experimental procedure. First, when the skin substitute moved downward with the motion of the sample gripper, the surgical needle was vertically fixed on a load cell and punctured the skin substitute with its tip, as shown in Fig. 3a. Then, the surgical suture was inserted into the drilled chamber at the end of the surgical needle, and the reversed sample gripper was set in the tensile tester. Subsequently, a small part of the surgical suture penetrated the skin substitute. The surgical suture was cut at the end of the surgical needle, and the short end of the surgical suture was attached to the load cell. The long end of the surgical suture was free as shown in Fig. 2b. Finally, the friction force was measured by the load cell with the upward movement of the sample gripper. The force and the corresponding curve were recorded automatically. An overview of the test conditions is given in Table 2. The measurement process

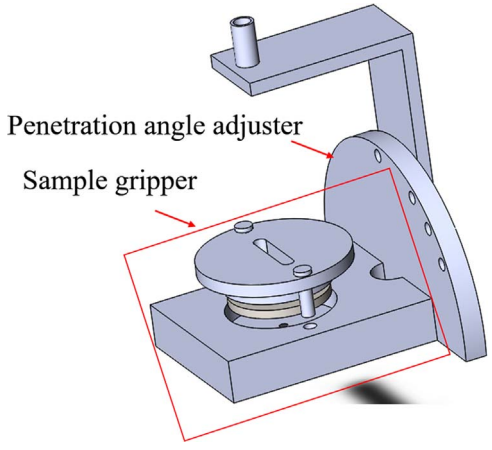

Fig. 2. Sample gripper and penetration angle adjuster.

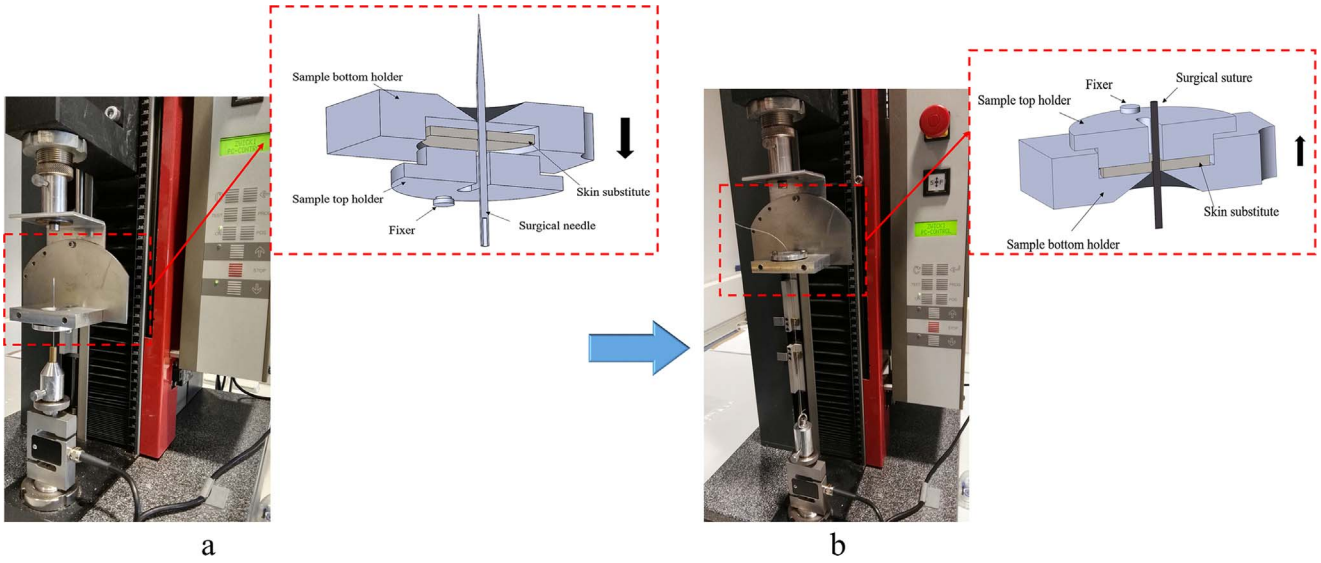

Fig. 3. Experimental procedure of penetration friction apparatus: (a) puncture procedure; (b) penetration procedure.

Table 2
Experimental parameters.

Test-related	Instructions
Equipment	Penetration friction apparatus
Diameter of gripper space	25 ± 0.5 mm
Diameter of cross hole	2 mm
Penetration angle	90°
Puncture velocity	60 mm/min
Puncture distance	10 mm
Penetration velocity	100 mm/min
Penetration distance	150 mm

ensured that every surgical suture penetrated the skin substitute once. Three repetitions of each sample were measured for each experimental setting.

2.1.3. Analysis of materials

The sample surface was analyzed with a laser confocal microscope (VK 9700 from KEYENCE, Japan) at magnifications of 10 × and 50 × . Surface images of three different samples of each size of the PGA surgical suture and skin substitute were obtained and the profile roughness parameters were determined. The roughness is presented in area properties (3D, S_a) instead of in line properties (2D, R_a), which can provide improved information on the surface aspects related to height.

Young's modulus of the polymer was measured by nano-indentation tests (Calahorra et al., 2015; He et al., 2006; Kinney et al., 1996). Young's modulus of each PGA multifilament surgical suture in the radial direction was measured by a Nano Indenter G200 from Keysight Technologies Inc. (USA) with a standard XP indentation head of 2 nm in diameter for the indenter, based on ISO 14577. Young's modulus of each surgical suture was calculated as the mean value of four measurements.

To fix the surgical suture, a thin thermoplastic resin adhesive film was coated on a heating metal support. A PGA surgical suture of 5 cm in length was placed horizontally on the heating metal support, and was then fixed to the surface of the support once the temperature of the thermoplastic resin adhesive had fallen to room temperature. Part of the surgical suture was embedded into the hard adhesive. The maximum force applied was 500 mN and the loading rate was 0.017 mN/s. The displacement resolution was 200 nm. A holding time of 10 s was established at the maximum displacement.

2.2. Prediction of the normal force

The insertion of a surgical suture involves radial expansion of the material. The proposed contact model assumes that normal force F_N is defined by the force to expand the planar crack from zero initial radius to a final surgical suture radius, as shown in Fig. 4. The surgical suture was regarded as an incompressible, elastic, isotropic fibre with a cylindrical geometry. The direction of F_N is perpendicular to the direction of the surgical suture motion. In order to better characterize the normal force on the surgical suture, a Hertzian contact model, FEM and UDM were involved.

2.2.1. Hertzian contact model

A Hertzian contact model (Johnson and Johnson, 1987; Marchand et al., 2012) was used to estimate the normal force F_N, although typically these models are accurate only for relatively small deformations. An idealized contact situation was assumed whereby the skin substitute was radially displaced and conformed around the inserted surgical suture. Furthermore, it was assumed that the normal force F_N subjected on the surgical suture was evenly distributed in a symmetrical way (Fig. 5a). Meanwhile, a reaction force F_r acted on the skin substitute (Fig. 5b), as shown in Eq. (1).

$$F_N = -F_r \tag{1}$$

The calculation of the force F_r was conducted using a Hertzian

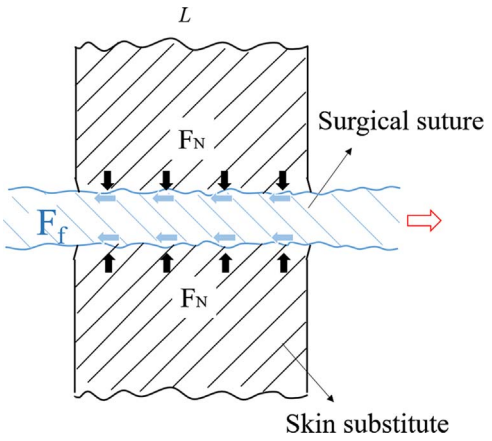

Fig. 4. Schematic representation of surgical sutures penetrating skin substitutes.

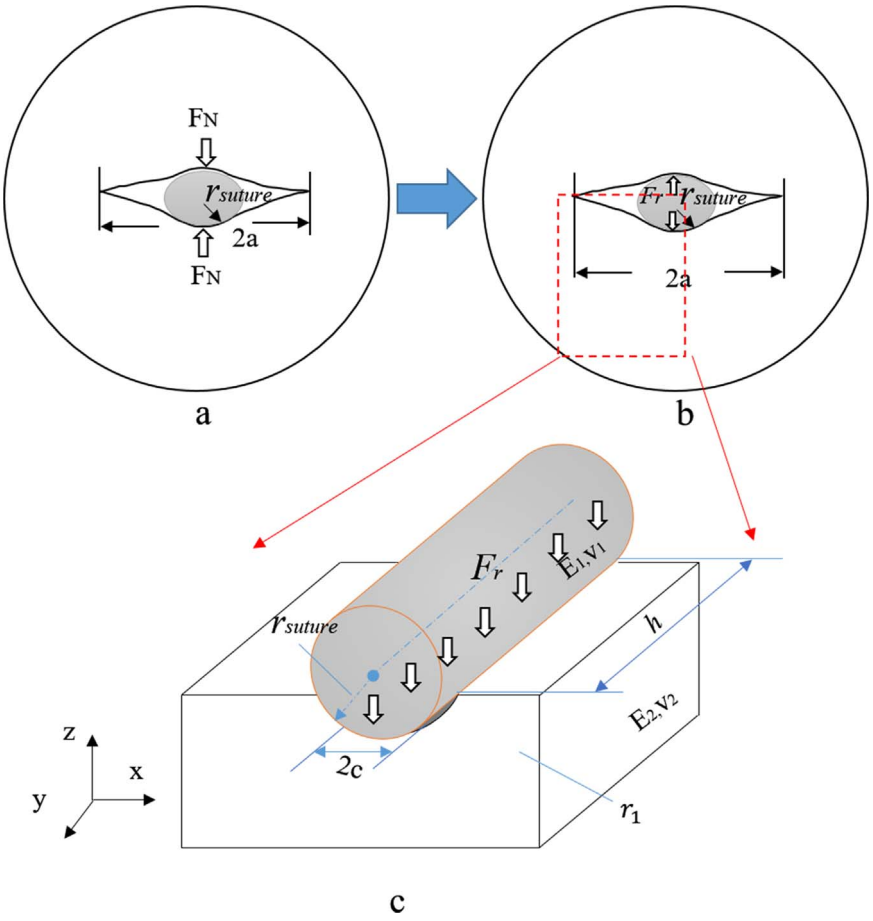

Fig. 5. (a) Steady-state penetration of skin substitute by surgical suture and (b) Equal and opposite forces worked on the skin substitute. (c) Contact of elastic sphere with an elastic half-space.

contact model for a cylinder-flat contact (Adams and Nosonovsky, 2000; Hanaor et al., 2015; Johnson and Johnson, 1987) as shown in Fig. 5c.

The half-width c of the contact area between the cylinder and flat in a Hertzian line contact is found using Eq. (2):

$$c = \sqrt{\frac{4F_r r}{\pi L E^*}} \tag{2}$$

$$\frac{1}{E^*} = \frac{1-\nu_1^2}{E_1} + \frac{1-\nu_2^2}{E_2} \tag{3}$$

$$\frac{1}{r} = \frac{1}{r_{suture}} + \frac{1}{r_1} \tag{4}$$

where F_r is the force acting on the surgical sutures; E^* is the reduced Young's modulus (refer to Eq. (3)); E_1, E_2 and ν_1, ν_2 are Young's moduli and Poisson's ratios for the surgical suture and skin substitute, respectively; r is the reduced radius of curvature (refer to Eq. (4)), and r_{suture} and r_1 are the radii of the curvature of the surgical suture and skin substitute, respectively; and h is the contact length. Young's modulus of the value shown in Table 3 and a Poisson's ratio of 0.4 were taken for the surgical suture.

In the contact condition, when the suture penetrates the skin and full contact occurs over the radius of the suture, the half-width $c = r_{suture}$. Being a flat, the radius of r_1 was infinitely great. Thus according to the above mentioned equations, F_N can be calculated as:

$$F_N = \frac{1}{4}\pi r L E^* \tag{5}$$

2.2.2. UDM and FEM

The normal force is also calculated based on a simplified elastic model, assuming uniaxial deformation (Casanova et al., 2014; White et al., 2011). In UDM, the value of F_N is defined as the product of normal stress σ and nominal contact area A_n (Sharp et al., 2009).

$$F_N = \sigma A_n \tag{6}$$

When a surgical suture inserted in a skin substitute cracks in a steady state, the nominal contact area A_n between the surgical suture and skin substitute is estimated with a finite-element approach using FEM. The normal stress σ is calculated by simplified elastic equations. The corresponding normal forces taken from the FEM calculations are presented in tabular form.

A steady-state penetration nominal contact area A_n was calculated. It was assumed herein that an initially closed crack of length $2a$, in the skin substitute of thickness L, which matched the one measured in the experiment, was opened to accommodate a cylindrical surgical suture with radius r, as shown in Fig. 6a and b. R was the diameter of the cross

Table 3
Young's modulus of PGA surgical sutures.

PGA surgical suture	1 #	0 #	2–0	3–0	4–0
Young's modulus (GPa)	0.48 ± 0.04	0.48 ± 0.05	0.48 ± 0.03	0.49 ± 0.06	0.49 ± 0.03

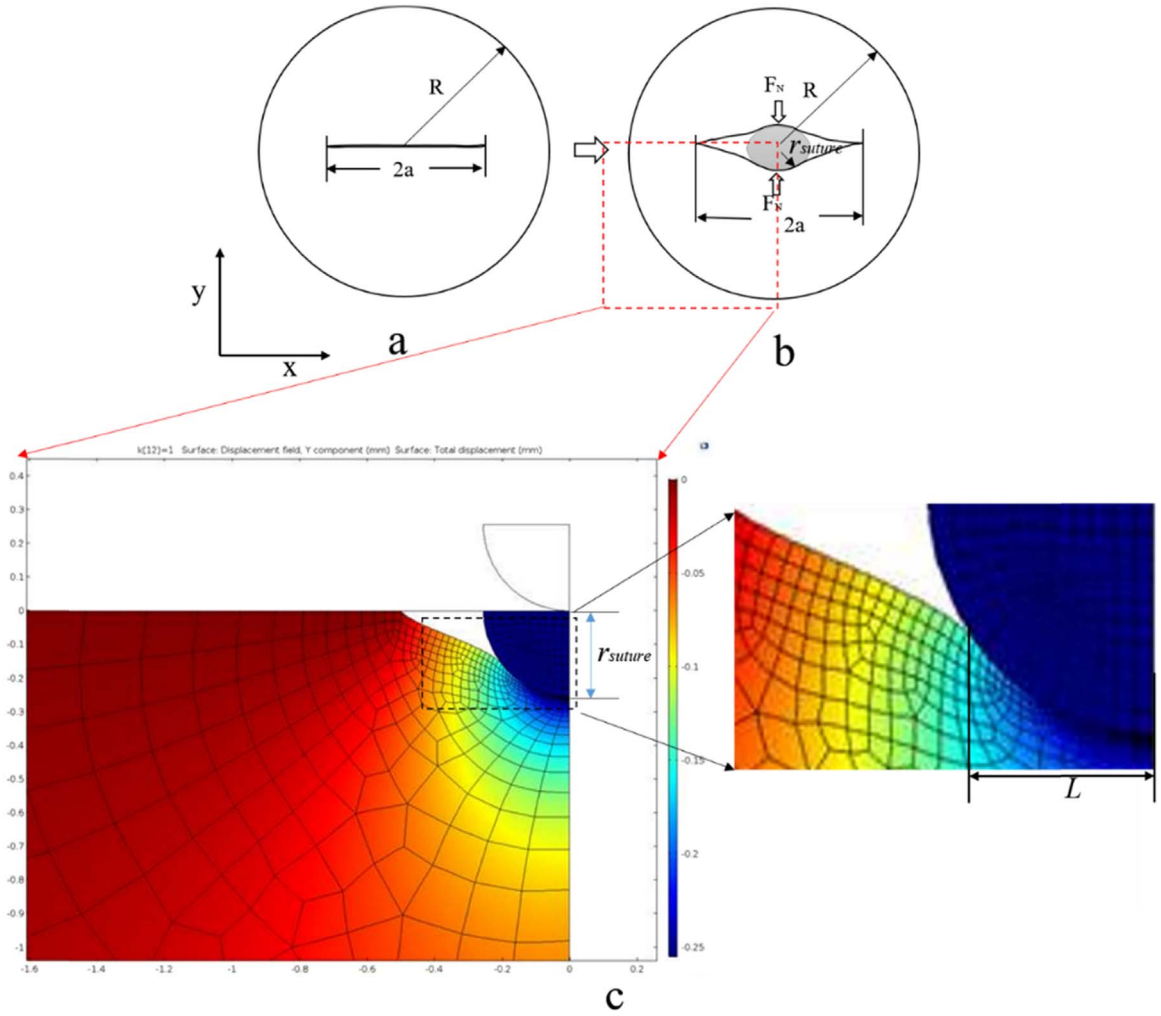

Fig. 6. Nominal contact predicted based on finite element simulation: (a) skin substitute with planar crack; (b) skin substitute with inserted surgical suture; (c) contact model simulated with FEM.

hole in the PFA. The main result is the contact length L, as indicated in Fig. 6. In the results depicted in Fig. 6, a was 0.42 ± 0.1 mm and R was 1 mm. Young's moduli of the skin substitute and surgical suture were 2.7 MPa and 470 MPa, respectively.

One-quarter of the contact was simulated on the basis of symmetry. In the simulated calculation, it was assumed that a displacement at the center of the crack, with fixed 2a length, was imposed on the center of the suture. This displacement is equal to half the diameter r_{suture} in the y-direction in the model to accommodate the suture as shown in Fig. 6c. The resulting contact lengths L as a function of the surgical suture sizes are summarized in Table 4. The nominal contact area A_n is the product of contact length L multiplied by 2 and the thickness of skin substitute h, as shown in Eq. (7):

$$A_n = 2hL \tag{7}$$

The normal stress σ was estimated using the following stress-strain relationship (Sharp et al., 2009), in a simplified way assuming a uniaxial linear elastic deformation:

$$\sigma = E^*\varepsilon \tag{8}$$

where E is the elastic modulus of the skin substitute and ε is the strain.

When the surgical suture was inserted into the skin substitute after puncturing by the surgical needle, the strain of the skin substitute could be assumed and the open planar crack of length 2a was approximated by an elliptical shape, as shown in Fig. 7a. The radius deformation of the skin substitute caused the normal force, as shown in Fig. 7b. In the elliptical shape, the semi-major radius was a (the half width of the planar crack). The semi-minor radius was r_{suture} (the radius of the surgical suture). The strain acting on the skin substitute was the ratio of the original length (y1) and the deformation (y2). Here, it will be assumed that y1 is equal to the radius of the cross hole in the PFA (R). Hence, ε in the x-direction was derived as in Eq. (9):

$$\varepsilon = \frac{y2}{y1} = \frac{r_{suture}}{a}\sqrt{\frac{a^2 - x^2}{R^2 - x^2}} \tag{9}$$

Therefore, the normal force F_N can be calculated by Eq. (10), using Eqs. (6)–(9) and by integrating the stresses required to cause the elliptically deformed shape over the total crack width.

$$F_N = 2EhL\frac{r_{suture}}{a}\int_0^a \sqrt{\frac{a^2 - x^2}{R^2 - x^2}}\,dx \tag{10}$$

Table 4
Contact length h and normal force estimated with a finite-element approach.

Diameter of surgical suture (mm)	Contact length (mm)	Normal Force (N)
.19	0.13	0.78
0.23	0.16	1.0
0.34	0.25	1.7
0.46	0.36	2.46
0.51	0.41	2.96

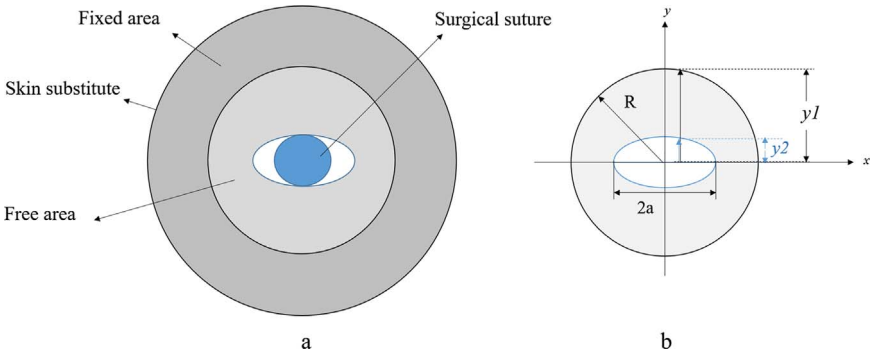

Fig. 7. Schematic of strain of skin substitute in penetration process: (a) skin substitute fixed in PFA with inserted surgical suture; (b) assumption of ellipse in skin substitute.

3. Results

In this part, the friction force between the surgical suture and skin substitute was investigated, and the effect of the surgical suture size on the friction force was estimated. All of the results below were obtained from repeated experiments.

3.1. Friction force and surface topography

In order to better understand the penetration process of a surgical needle and suture, the inserted states of the surgical needle and surgical suture in a skin substitute are observed in Fig. 8. First, the needle pierced and was inserted into the skin substitute (refer to Fig. 8a and b). The sharp needle punched through the skin substitute, forming a planar crack with the tip, and the crack surfaces were wedged open. The same phenomena were observed by Shergold (Shergold and Fleck, 2004). After the surgical needle was removed, the planar track closed tightly owing to the resilience of the skin substitute (refer to Fig. 8c and d). Second, the surgical suture penetrated the surgical needle track in the skin substitute (refer to Fig. 8e and f). After the surgical suture penetrated the skin substitute, wear debris that originated from the skin substitute was observed near the planar track (refer to Fig. 8g and h).

The size of the surgical suture significantly influences the friction force when surgical sutures penetrate the same needle crack. Fig. 9. shows the friction force of different sizes of PGA multifilament surgical sutures (from 0.19 mm to 0.51 mm) when penetrating the track punched by a 1# surgical needle in skin substitute, at a velocity of 100 mm/min. In this figure, a trend is observed in that the friction force increased considerably (from 0.36 N to 1.15 N) as the diameters of the PGA multifilament surgical sutures increased.

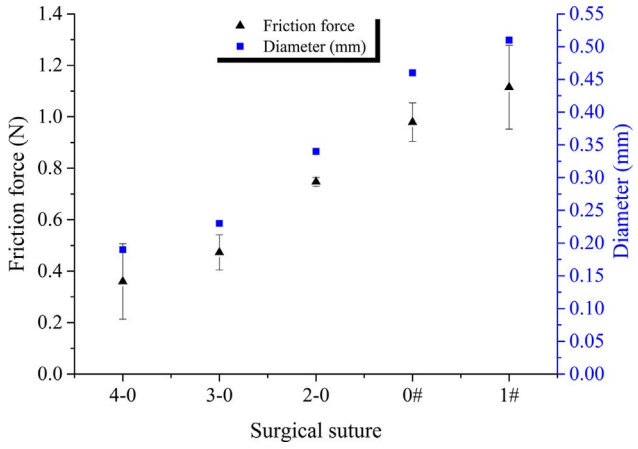

Fig. 9. Friction force of PGA multifilament surgical sutures with different diameters.

3.2. Normal force and COF

The nominal contact area and normal force calculated by the three models are shown in Fig. 10. Fig. 10a and b show that the nominal

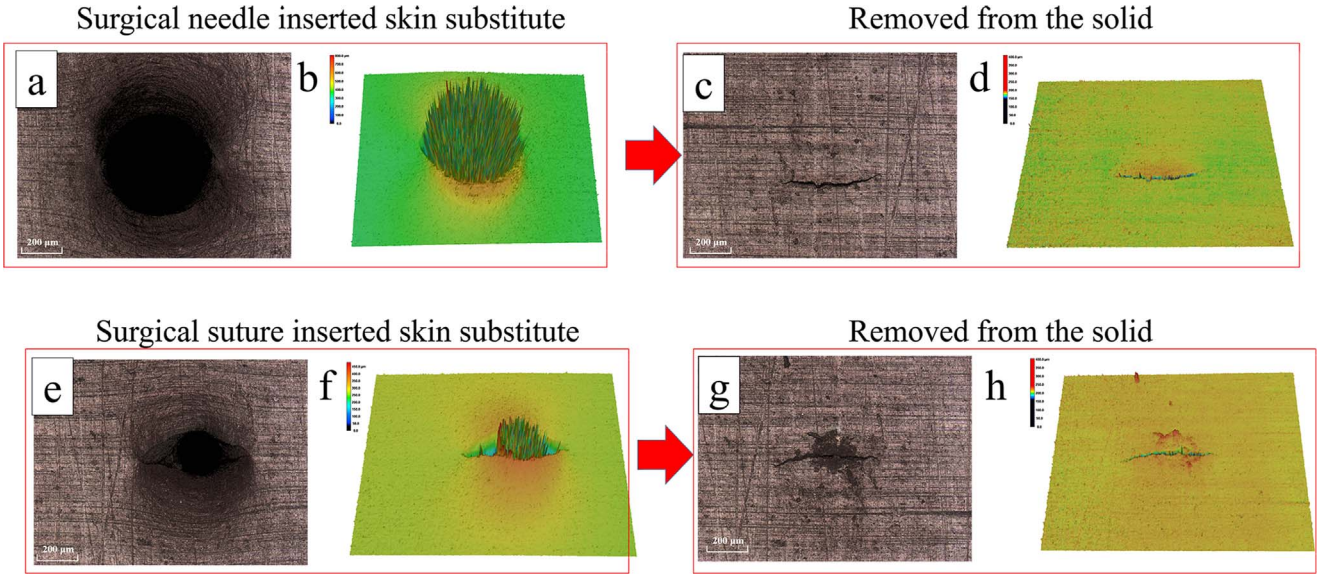

Fig. 8. Laser confocal images of inserted states of surgical needle and surgical suture in skin substitute: (a, b) surgical needle inserted into skin substitute; (c, d) surgical needle removed from skin substitute; (e, f) surgical suture inserted into skin substitute; (g, h) surgical suture removed from skin substitute.

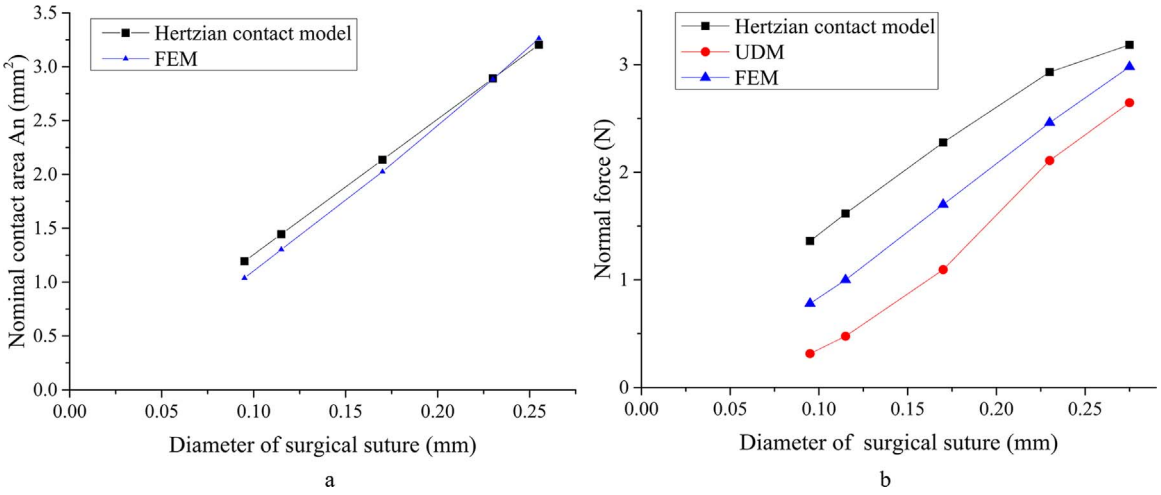

Fig. 10. (a) Nominal contact area and (b) normal force derived from finite element model, uniaxial deformation model and Hertzian contact model.

contact area and normal force between the surgical suture and skin substitute increase as the surgical suture size increase for all three models. It can be seen that the nominal contact area and normal force estimated by UDM and FEM were less than those estimated by the Hertzian contact model (refer to Fig. 10a). The normal force predicted by FEM was much lower than that estimated by the Hertzian model and was quite similar to that of UDM, especially at larger suture diameters (refer to Fig. 10b).

According to the friction of fibrous materials, the shear strength and real contact area are important factors that influence the friction performance of fibrous materials. As the diameters increase, the nominal contact area increases (refer to Fig. 10a). The real contact area is relative to the nominal contact area and minor differences occurr between them. Hence, the real contact area also increased as the diameter of the surgical suture increased. Moreover, an increase in the diameter of the surgical suture led to an increase in the displacement of the skin substitute, leading to a higher normal force. A higher normal force does not necessarily result in a proportionally higher friction force, as can be seen in Fig. 10.

In order to understand the frictional performance of a surgical suture sliding through a skin substitute, the relationship between the friction force and normal force was investigated using an experimental setup. Fig. 11 shows that the coefficient of friction (COF) predicted by FEM, defined as the quotient of the friction force and normal force, decreased from 0.92 to 0.75 as the normal force increased from 0.78 to 2.98 N. However, the COF prediction based on the uniaxial deformation model decreased from 2.29 to 0.42 as the normal force increased from 0.31 to 2.65 N. Compared with the above two models, the COF prediction based on the Hertzian contact model ranged from 0.26 to 0.35 as the normal force increased from 1.36 to 3.18 N. A similar curved trend with the uniaxial deformation model was reported by Ramkumar et al. (2004, 2003), highlighting the deviations from Amontons' law of friction in the case of polymeric fibrous materials.

An alternative relation, given the observed dependence of the frictional force on the normal force, has been the subject of many investigations (Bowden and Young, 1951; Gralén et al., 1953b; Lincoln, 1952; Viswanathan, 1966). The results from previous studies have shown that the power-law relationship as given in Eq. (11) can be used to represent the relationship between the friction forces and normal force for fibrous materials.

$$F_f = kF_N^n \tag{11}$$

where k and n are the empirical fitting parameters. The value of k depends on the sliding interaction and the materials (Bowden and Young, 1951; Howell and Mazur, 1953). The value of k was found to be similar to that of the parameter μ. The index n, with values of the n exponent

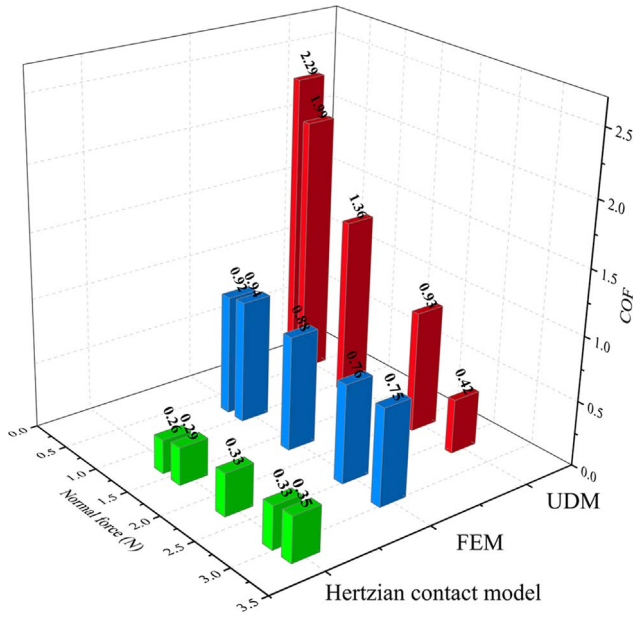

Fig. 11. Coefficient of friction for different surgical suture sizes and corresponding normal forces.

between 0.67 and 1.1 (van Kuilenburg, 2013), is governed by the viscoelastic and shearing properties of the junctions as a function of the normal force (El Mogahzy and Gupta, 1993b).

The coefficient of friction (μ_{equ}) can be deduced from Eq. (12) and is given by

$$\mu_{equ} = kF_N^{1-n} \tag{12}$$

where μ_{equ} is the equivalent Coulomb coefficient of friction. From Eq. (12), it can be seen that the calculated μ_{equ} does not remain constant for load-dependent material behavior. With an increase in the normal force, μ_{equ} of a friction surgical suture sliding through the skin substitute decreases.

Hence, the COF derived from UDM gives reasonable results when describing the frictional response of a surgical suture sliding through a skin substitute, given the power- law type of relation in which it results. The COF found for various skin sliding interactions might vary over a large range, i.e, from 0.02 to 2.62 depending on the tribosystem see (Darden and Schwartz, 2009; van Kuilenburg, 2013). Values for hydrated skin typically reach 1.6 (Darden and Schwartz, 2009). The COF predicted by UDM and based on measurements for a skin substitute

seems to be in a reasonable range for the penetration friction condition.

4. Discussion

In the suturing process (refer to Fig. 8), first, the needle penetrates the tissue and creates a freshly formed counter surface with a damaged tissue. Second, the surgical suture connected to the surgical needle penetrates through the skin substitute followed by the surgical needle. The frictional performance of the surgical suture is influenced by mechanical and surface properties and the contacting materials as well as by the operational conditions.

In a penetration contact model, the diameter of the surgical needle is related to the length of the crack of the skin substitute. This is a significant factor influencing the normal force. In order to remove the negative influence of different crack sizes and focus on the influence of the surgical suture size, the same size of surgical sutures (1#) was used to pull the surgical sutures through a skin substitute. From Fig. 9, it can be seen that the friction force increased as the diameter of the surgical suture increased. This may be because increasing the diameter of surgical sutures led to an increase in the normal force, thus leading to a higher friction force. As the surgical suture diameter increased, more skin substitute in the vicinity of the suture was displaced and compressed. The resilience of the compressed skin substitute generated more normal force. Hence, under the same crack conditions, the magnitude of the radial force depended on the diameter of the surgical sutures.

From Fig. 9, it also can be seen that the values of the error bar of a 2–0 PGA multifilament surgical suture were less than those of other sizes of surgical sutures. This may result from the effect of the diameter ratio of surgical needle and suture. When different sizes of sutures penetrated tissue following the same needles, a smaller surgical suture would cause more cut trauma and a larger surgical suture would cause more friction. A previous study (Zhang et al., 2017a) found that, when the diameter ratio of surgical needle and suture was 2.5, trauma and friction force were balanced. From the measurement of Fig. 8, the length of the crack of skin substitute puncture of the needle is equal to the diameter of the surgical needle. The diameter ratio between the 2–0 PGA multifilament surgical suture and the 1# surgical needle was close to 2.5.

In order to generate guidelines for the development of surgical sutures with desirable tribological performance, the following suggestions are proposed: (1) When the diameter ratio of the surgical needle and suture is in an appropriate range, this is more representative of real life. (2) The coefficient of friction could be calculated by the friction force, which is measured by the PFA and the normal force, which is predicted by UDM.

The friction performance of surgical sutures can be estimated by the above approach. By providing the surgeon with accurate frictional parameters of surgical sutures, the medical risk caused by the selection of unsuitable surgical sutures can be reduced, thereby improving the patient's postoperative recovery.

5. Conclusion

The friction force of different sizes of PGA surgical sutures was measured by means of a penetration friction apparatus (PFA). The friction force F_f was measured by the PFA with a penetration angle of 90°, and the normal force F_N was predicted by a finite element model, a Hertzian model and a simplified uniaxial deformation model.

1. The results indicated that the penetration friction force increased from 0.35 to 1.15 N as the diameter of the PGA multifilament surgical suture increased from 0.19 to 0.55 mm.
2. The nominal contact area and normal force between the surgical suture and skin substitute increased as the diameters of the surgical sutures increased for the Hertzian, UDM linear elastic and FEM model.
3. The relationship between the friction force and normal force decreased from 2.29 to 0.42 as the normal force that was predicted with the uniaxial deformation model increased from 0.31 to 2.56 N.
4. The COF predicted by the uniaxial deformation model and based on measurements for the skin substitute seems to be in a reasonable range for the penetration friction condition.

Acknowledgements

The authors would like to thank Sheng Zhang from Micro/Nano Technology Center, Tokai University, Erik de Vries, Walter Lette and Yuxin Zhou in the laboratory for surface technology and tribology for their attention and assistance.

The authors are grateful to Marie Curie CIG (Grant no. PCIG10-GA-2011-303922), the Shanghai Natural Science Foundation (Grant no. 17ZR1442100), and the Shanghai Municipal “Science and Technology Innovation Action Plan” International Cooperation Project (Grant no. 15540723600), and the Innovation Fund of Precision Medicine (Grant no. 2016A003) for their financial support.

References

Adams, G., Nosonovsky, M., 2000. Contact modeling—forces. Tribology Int. 33, 431–442.
Bloom, B.S., Goldberg, D.J., 2007. Suture material in cosmetic cutaneous surgery. J. Cosmet. Laser Ther. 9, 41–45.
Bowden, F.P., Young, J.E., 1951. Friction of diamond, graphite, and carbon and the influence of surface films. Proc. R. Soc. Lond. Ser. A. Math. Phys. Sci. 208, 444–455.
Calahorra, Y., Shtempluck, O., Kotchetkov, V., Yaish, Y., 2015. Young's modulus, residual stress, and crystal orientation of doubly clamped silicon nanowire beams. Nano Lett. 15, 2945–2950.
Casanova, F., Carney, P.R., Sarntinoranont, M., 2014. In vivo evaluation of needle force and friction stress during insertion at varying insertion speed into the brain. J. Neurosci. Methods 237, 79–89.
Darden, M.A., Schwartz, C.J., 2009. Investigation of skin tribology and its effects on the tactile attributes of polymer fabrics. Wear 267, 1289–1294.
El Mogahzy, Y.E., Gupta, B.S., 1993a. Friction in fibrous materials part II: experimental study of the effects of structural and morphological factors. Text. Res. J. 63, 219–230.
El Mogahzy, Y.E., Gupta, B.S., 1993b. Friction in fibrous materials: part II: experimental study of the effects of structural and morphological factors. Text. Res. J. 63, 219–230.
Gao, X., Wang, L., Hao, X., 2015. An improved Capstan equation including power-law friction and bending rigidity for high performance yarn. Mech. Mach. Theory 90, 84–94.
Ghosh, A., Patanaik, A., Anandjiwala, R.D., Rengasamy, R.S., 2008. A study on dynamic friction of different spun yarns. J. Appl. Polym. Sci. 108, 3233–3238.
Gralén, N., Olofsson, B., Lindberg, J., 1953a. Measurement of friction between single fibers. Text. Res. J. 23, 623–629.
Gralén, N., Olofsson, B., Lindberg, J., 1953b. Measurement of friction between single fibers part VII: physicochemical views of interfiber friction. Text. Res. J. 23, 623–629.
Gralen, N., 1952. Friction between single fibres. Proc. R. Soc. Lond. Ser. A, Math. Phys. Sci. 491–495.
Gralen, N., Lindberg, J., 1948. Measurement of friction between single fibers, Part II: frictional properties of wool fibers measured by the fiber-Twist method. Text. Res. J. 18, 287–301.
Gupta, B.S., Wolf, K.W., Postlethwait, R.W., 1985. Effect of suture material and construction on frictional properties of sutures. Surg. Gynecol. Obstet. 161, 12–16.
Hanaor, D.A.H., Gan, Y., Einav, I., 2015. Contact mechanics of fractal surfaces by spline assisted discretisation. Int. J. Solids Struct. 59, 121–131.
He, L.H., Fujisawa, N., Swain, M.V., 2006. Elastic modulus and stress–strain response of human enamel by nano-indentation. Biomaterials 27, 4388–4398.
Howell, H.G., Mazur, J., 1953. Amontons' Law and fibre friction. J. Text. Inst. Trans. 44, T59–T69.
Johnson, K.L., Johnson, K.L., 1987. Contact Mechanics. Cambridge University Press.
Kinney, J.H., Balooch, M., Marshall, S.J., Marshall Jr, G.W., Weihs, T.P., 1996. Hardness and young's modulus of human peritubular and intertubular dentine. Arch. Oral. Biol. 41, 9–13.
Lincoln, B., 1952. Frictional and elastic properties of high polymeric materials. Br. J. Appl. Phys. 3, 260.
Marchand, A., Das, S., Snoeijer, J.H., Andreotti, B., 2012. Capillary pressure and contact line force on a soft solid. Phys. Rev. Lett. 108, 094301.
McBride, T.E., 1965. Development of an instrument to measure friction of textile fibers.
Misra, S., Ramesh, K., Okamura, A., 2008. Modeling of tool-tissue interactions for computer-based surgical simulation: a literature review. Presence 17, 463–491.
Ramkumar, S.S., Rajanala, R., Parameswaran, S., Paige, R., Shaw, A., Shelly, D.C., Anderson, T.A., Cobb, G.P., Mahmud, R., Roedel, C., Tock, R.W., 2004. Experimental verification of failure of Amontons' law in polymeric textiles. J. Appl. Polym. Sci. 91, 3879–3885.
Ramkumar, S.S., Shastri, L., Tock, R.W., Shelly, D.C., Smith, M.L., Padmanabhan, S., 2003. Experimental study of the frictional properties of friction spun yarns. J. Appl.

Polym. Sci. 88, 2450–2454.
Robins, M., W Rennell, R., Arnell, R, D., 2000. The friction of polyester textile fibres.
Sharp, A.A., Ortega, A.M., Restrepo, D., Curran-Everett, D., Gall, K., 2009. In vivo penetration mechanics and mechanical properties of mouse brain tissue at micrometer scales. IEEE Trans. Biomed. Eng. 56, 45–53.
Shergold, O.A., Fleck, N.A., 2004. Mechanisms of deep penetration of soft solids, with application to the injection and wounding of skin. Proc. R. Soc. Lond. A: Math., Phys. Eng. Sci. R. Soc. 3037–3058.
Shergold, O.A., Fleck, N.A., 2005. Experimental investigation into the deep penetration of soft solids by sharp and blunt punches, with application to the piercing of skin. J. Biomech. Eng. 127, 838–848.
Shergold, O.A., Fleck, N.A., Radford, D., 2006. The uniaxial stress versus strain response of pig skin and silicone rubber at low and high strain rates. Int. J. Impact Eng. 32, 1384–1402.
Tu, C.-F., For, T., 2004. A study of fiber-capstan friction. 1. Stribeck curves. Tribology Int. 37, 701–710.
Tu, C.-F., Fort, T., 2004. A study of fiber-capstan friction. 2. stick–slip phenomena. Tribology Int. 37, 711–719.
van Kuilenburg, J., 2013. A Mechanistic Approach To Tactile Frictio (Ph.D. thesis). University of Twente, The Netherlands.
Viswanathan, A., 1966. Frictional forces in cotton and regenerated cellulose fibres. J. Text. Inst. Trans. 57, T30–T41.
White, E., Bienemann, A., Malone, J., Megraw, L., Bunnun, C., Wyatt, M., Gill, S., 2011. An evaluation of the relationships between catheter design and tissue mechanics in achieving high-flow convection-enhanced delivery. J. Neurosci. Methods 199, 87–97.
Zhang, G., Ren, T., Lette, W., Zeng, X., van der Heide, E., 2017a. Development of a penetration friction apparatus (PFA) to measure the frictional performance of surgical suture. J. Mech. Behav. Biomed. Mater. 74, 392–399.
Zhang, G., Ren, T., Zeng, X., Van Der Heide, E., 2017b. Influence of surgical suture properties on the tribological interactions with artificial skin by a capstan experiment approach. Friction 5, 87–98.